Article

Sensitivity of Tropical Cyclone Idai Simulations to Cumulus Parametrization Schemes

Mary-Jane M. Bopape [1,*], Hipolito Cardoso [2], Robert S. Plant [3], Elelwani Phaduli [1], Hector Chikoore [4], Thando Ndarana [5], Lino Khalau [6] and Edward Rakate [7]

1   South African Weather Service, Private Bag X097, Pretoria 0001, South Africa; elelwani.phaduli@weathersa.co.za
2   Instituto Nacional de Meteorologia, Rua de Mukumbura, 164, C.P. 256 Maputo, Mozambique; hipolito_c@inam.gov.mz
3   Department of Meteorology, Earley Gate, University of Reading, Reading RG6 6BB, UK; r.s.plant@reading.ac.uk
4   Department of Geography and Environmental Management, North-West University, Vanderbijlpark 1900, South Africa; 32945280@nwu.ac.za
5   Department of Geography, Geoinformatics and Meteorology, University of Pretoria, Pretoria 0002, South Africa; thando.ndarana@up.ac.za
6   Mozambique Research and Education Network, 770 Patrice Lumumba Avenue, C.P. 256 Maputo, Mozambique; lino.khalau@morenet.ac.mz
7   National Integrated Cyber-Infrastructure System, Council for Scientific and Industrial Research, Brummeria, Pretoria 0184, South Africa; ERakate@csir.co.za
*   Correspondence: mary-jane.bopape@weathersa.co.za

Abstract: Weather simulations are sensitive to subgrid processes that are parameterized in numerical weather prediction (NWP) models. In this study, we investigated the response of tropical cyclone Idai simulations to different cumulus parameterization schemes using the Weather Research and Forecasting (WRF) model with a 6 km grid length. Seventy-two-hour (00 UTC 13 March to 00 UTC 16 March) simulations were conducted with the New Tiedtke (Tiedtke), New Simplified Arakawa–Schubert (NewSAS), Multi-Scale Kain–Fritsch (MSKF), Grell–Freitas, and the Betts–Miller–Janjic (BMJ) schemes. A simulation for the same event was also conducted with the convection scheme switched off. The twenty-four-hour accumulated rainfall during all three simulated days was generally similar across all six experiments. Larger differences in simulations were found for rainfall events away from the tropical cyclone. When the resolved and convective rainfall are partitioned, it is found that the scale-aware schemes (i.e., Grell–Freitas and MSKF) allow the model to resolve most of the rainfall, while they are less active. Regarding the maximum wind speed, and minimum sea level pressure (MSLP), the scale aware schemes simulate a higher intensity that is similar to the Joint Typhoon Warning Center (JTWC) dataset, however, the timing is more aligned with the Global Forecast System (GFS), which is the model providing initial conditions and time-dependent lateral boundary conditions. Simulations with the convection scheme off were found to be similar to those with the scale-aware schemes. It was found that Tiedtke simulates the location to be farther southwest compared to other schemes, while BMJ simulates the path to be more to the north after landfall. All of the schemes as well as GFS failed to simulate the movement of Idai into Zimbabwe, showing the potential impact of shortcomings on the forcing model. Our study shows that the use of scale aware schemes allows the model to resolve most of the dynamics, resulting in higher weather system intensity in the grey zone. The wrong timing of the peak shows a need to use better performing global models to provide lateral boundary conditions for downscalers.

Keywords: tropical cyclone Idai; cumulus parameterization; WRF model; flooding

1. Introduction

Tropical cyclones are low-pressure systems that develop over warm tropical and subtropical waters [1]. When they make landfall, these systems can result in very heavy rainfall, storm surges and flooding. In the United States, they were found to account for one third of the trend in extreme precipitation [2]. These systems occur in both the Northern and Southern Hemispheres with similar intensity. They are associated with high sea surface temperatures, and thus exhibit seasonality centred around the warmer months [3]. Southeast Africa is also impacted by these systems, with Madagascar and Mozambique being the two countries that experience the most damage caused by tropical cyclones which develop in the South West Indian Ocean (SWIO) basin [4,5]. Mozambique is considered the most vulnerable to these systems because 39% of its population lives below 100 m elevation [6].

According to Mavume et al. [7], 16 tropical cyclones made landfall over Mozambique during the period 1980–2007. A notable tropical cyclone that developed during the period is Eline which initiated in the eastern Indian ocean where it was named Leon. The system was renamed Eline when it entered the SWIO basin. Eline made landfall on Madagascar, with a second landfall over Mozambique, and its remnants tracked farther west into Southern Africa resulting in rainfall over a number of countries including Namibia [8]. Chikoore et al. [5] reported on the January–March 2012 tropical cyclone season in which five systems either developed or were drawn into the Mozambique Channel. Another notable event was tropical cyclone Dineo whose remnants filled the Gaborone Dam in Botswana in February 2017 [9], and also severely impacted vulnerable communities in southern Zimbabwe[10]. More cyclones have made landfall in the recent past with category 4 tropical cyclones Idai and Kenneth making landfall in Mozambique during the 2018/2019 summer season [11]. Tropical storm Chalane and category 2 cyclones Eloise and Guambe made landfall in Mozambique during the 2020/2021 austral summer season. Tropical cyclone Jobo made a rare landfall over Tanzania in April 2021. According to Malherbe et al. [12], the frequency of tropical cyclones in the SWIO is projected to decrease towards the end of the 21st century, with a northward migration due to the strengthening of the subtropical ridge of high pressure.

The current study focuses on tropical cyclone Idai, an intense category 4 storm associated with very strong winds [13] which caused devastation in Mozambique, Zimbabwe and Malawi. The event was so devastating that the World Meteorological Organization (WMO) sent a mission to Mozambique to investigate the state of affairs in relation to weather forecasting, response, and impacts associated with the event [14]. According to the ensuing WMO report, over 600 lives were lost whilst over 1600 people were injured and over 1.8 million people were affected in Mozambique. The event resulted in a cholera outbreak with over 6500 confirmed cases, which was subsequently contained by a vaccination programme of over 800,000 people [15]. The event also impacted the power grid in Southern Africa due to damaged infrastructure in Mozambique as the country exports electricity to the neighbouring countries [16]. Land degradation was indicated by a notable decrease in the Normalized Difference Vegetation Index (NDVI) following the event [17]. In Zimbabwe, 270,000 people were affected and 340 lives were lost, while many lost their homes and livelihoods. School and agriculture infrastructure was also damaged [18].

Responses to extreme weather events ahead of an event or humanitarian relief efforts after the event can be impacted by social, economic and political factors, as was found in Zimbabwe following Idai [19]. One of the ways to reduce vulnerability to weather extremes is through the use of weather forecasts [20] to support responses before the event occurs. Forecasting weather with a lead time that goes beyond nowcasting relies on the use of Numerical Weather Prediction (NWP) models [21]. A number of studies have considered the performance of global and regional models for forecasting tropical cyclones that develop in the SWIO basin. Reason and Keibel [8] for example, compared forecasts of tropical cyclone Eline issued by tropical cyclone Regional Specialised Meteorological Centre (RSMC) La Réunion (Météo France) and by the Mauritius Meteorological Services

who rely on UK Met Office (UKMO) and Méteo France NWP models, as well as rainfall forecasts from the then South African Weather Bureau (SAWB). They found that the issued forecasts did provide useful information, especially for the track and landfall position of Eline, although there were some errors in the forecast speed and intensity of the storm. Dyson and Van Heerden [22] showed that the SAWB Eta model captured the geographical distribution of rainfall in the northeastern parts of South Africa during two heavy rainfall events in February 2000 including Eline, but that rainfall totals were underestimated by some 50%.

Chikoore et al. [5] studied the performance of models made available through the WMO Severe Weather Forecasting Demonstration Project (SWFDP) when simulating two tropical cyclones in 2012—Dando and Irina. The models underestimated Dando's precipitation, but overestimated that of Irina, and this was associated with the missed forecasts of tropical cyclone tracks by the models. Moses and Ramotonto [9] compared two global models, those of the European Centre for Medium-Range Weather Forecasts (ECMWF) Integrated Forecasting System (IFS) and of the National Center for Environmental Prediction (NCEP) Global Forecast System (GFS), when forecasting tropical cyclone Dineo. The study found that IFS outperformed the GFS in capturing the maximum rainfall values, location and intensity of the storm, while GFS performed better with the location of maximum rainfall, the location of a cloud band associated with the storm and overall rainfall amount. Some of the challenges mentioned above in forecasting tropical cyclones may be associated with limited observations for data assimilation purposes, or to shortcomings in models themselves, including the treatments of subgrid processes that must be parameterized.

Cumulus parameterization schemes are thought to be associated with much of the uncertainty in weather and climate simulations [23]. There are many cumulus schemes available in the research community, and a number of studies have investigated the sensitivity of different types of events to these schemes, including simulations of tropical cyclones, e.g., [24–26]. These climatological studies based on 2, 10, or 30 years of data found that the simulated frequency, intensity, cyclone track, and associated rainfall differ amongst the different convection schemes. Radhakrishnan and Balaji [27] studied the impact of different physics settings in the Weather Research and Forecasting (WRF) model when simulating tropical cyclone Jal and found the best suite for tracks is not best for intensity. The study also found that tracks were sensitive to the cumulus, planetary boundary layer, microphysics and long-wave radiation parameterizations, while intensity was found to be primarily sensitive to the cumulus scheme chosen. Davis [28] showed that resolution also has an impact on the simulated intensity of storms, with models using a grid spacing of 0.25° or less, expected to underestimate the number of category 4 and 5 storms.

As computational resources improve, the model resolution that organisations can afford increases. Although this can often prove beneficial, increases in resolution can also present scientific challenges to the meteorological community. In particular, some parameterization schemes may become obsolete if they rely upon assumptions that no longer hold at the higher resolution. The term "grey zone" is becoming increasingly used to describe scales at which the length scale of the event being simulated is similar to the grid length of the model [29,30]. Some of the newer parameterization schemes were developed in a way that allows their behaviour to adapt with changing resolution, and these are called scale aware schemes, e.g., [31,32]. Somses et al. [33] and Champion and Hodges [34] showed that switching off the convection scheme when a grid length of less than 5 km is used results in higher rainfall intensity being simulated. Furthermore, Steeneveld and Peerlings [29] indicated that the use of scale-aware schemes is beneficial for the representation of deep convection in the grey zones. Our study aimed to investigate the performance of different convection schemes in the grey zone when simulating a tropical cyclone. The next section describes the methodology, model and data used in the study, and the event itself is described in Section 3, while results of simulations are presented in Section 4, and summary and conclusions are discussed at the end.

2. Model, Data and Simulations

The experiments in this study were conducted using the Weather Research and Forecasting (WRF) version 4.1.2 model [35]. WRF is a non-hydrostatic model that can be used to produce operational forecasts as well as for research purposes for a range of space and timescales from inertial subranges to synoptic scales. Model prognostic variables include the vertical and horizontal wind components, cloud microphysical quantities, potential temperature, geopotential and surface pressure of dry air. WRF is a user-friendly open source model which is used in a number of countries worldwide [36] as well as in SADC countries to produce operational forecasts [37]. The model is officially supported by the National Center for Atmospheric Research (NCAR) [36]. It includes a wide range of physics options [35], which facilitates studies such as the current one, investigating sensitivities of simulations to different schemes. That said, the availability of many schemes can also come with the disadvantage that scientists would have difficulty selecting the best scheme for their area and event type of interest. The simulations considered here are described in Section 2.1, followed by the convection schemes used in the study (Section 2.2), the observation data used (Section 2.3), and finally, the verification measures chosen (Section 2.4).

2.1. Simulations

The model domain is defined in the Mercator projection with a 6 km grid length and centred around 20° S and 36.50° E. There is no agreed resolution for which clouds are considered fully resolved [38], where the convection scheme needs to be switched off. For example, Weisman et al. [39] concluded that a grid length of 4 km is cloud resolving because bulk dynamics of squall lines are captured, Roberts [40] recommended only switching off the convection schemes with grid length of around 1 km, while according to Bryan et al. [41] clouds are only resolved when the grid length used is of order 100 m. The resolution in this study was selected to be within the regime where there is consensus amongst scientists regarding the need to use convection schemes. At the same time, the resolution is high enough to be in the range suitable for regional operational NWP models, based on available computational resources and the resolution of global NWP models. The full domain is shown in Figure 1. The simulations are performed for 72 h, from 00 UTC 13 March to 00UTC 16 March 2019. The initial and boundary conditions were taken from the NCEP GFS [42], with lateral boundary condition updates every 3 h of simulation time. The GFS data have a horizontal grid spacing of 0.25°. The GFS simulated track, maximum wind speed and minimum sea level pressure generated using the Geophysical Fluid Dynamics Lab (GFDL) Vortex tracker (https://dtcenter.org/community-code/gfdl-vortex-tracker (accessed on 11 June 2021)) are also presented in the study. The WRF model output is written for every hour.

All the simulations were conducted using the tropical suite physics option due to the location of our domain in the lower latitudes [43,44]. The suite uses the rapid radiative transfer model (RRTM) for the parametrization of short- and long-wave radiation [45], the WRF Single Moment Single Moment 6-class microphysical scheme (WSM6) [46] and the Yonsei University (YSU) planetary boundary layer (PBL) scheme [47]. The standard cumulus scheme used in the tropical suite is the new Tiedtke scheme [48–50]. Since the aim of this study was to test different cumulus schemes, we summarised the main features of the four other selected schemes below, alongside those of the new Tiedtke scheme. We also performed a simulation with no cumulus scheme activated, so that all convection occurs through the model's dynamics. Other physics choices were kept the same in all WRF simulations. The selected time control, domain and physics setting are shown in Appendix A.

Domain, topography & Idai track
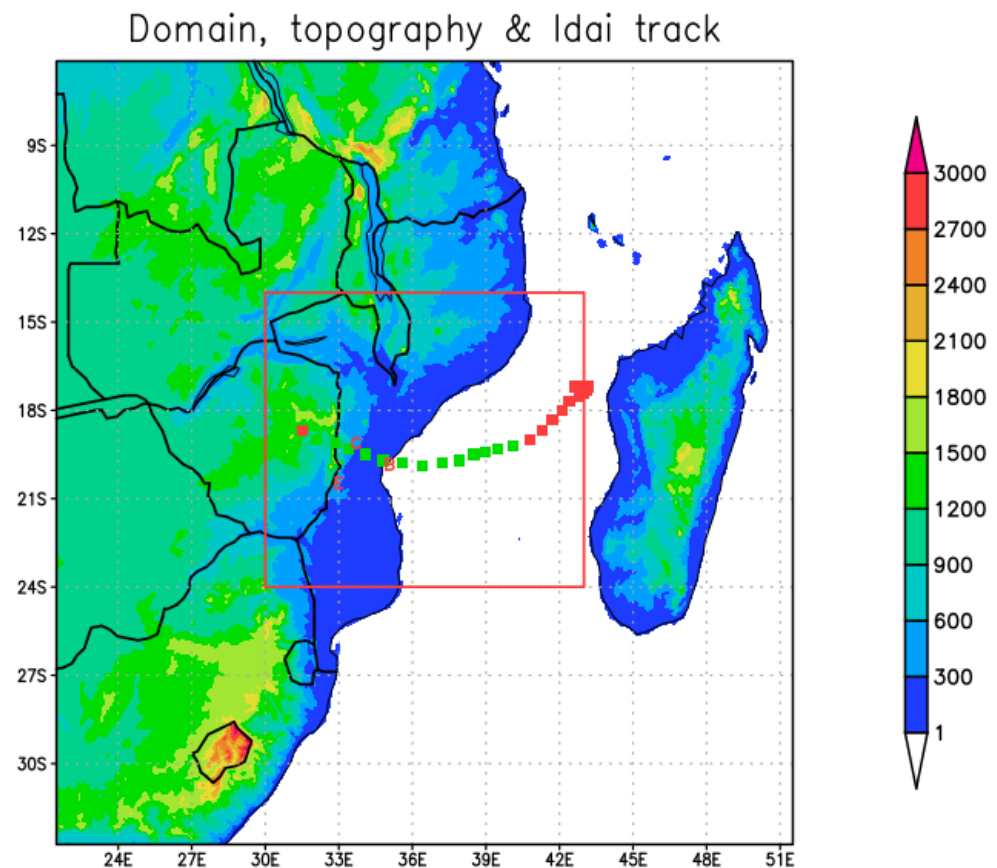
Figure 1. The simulation domain, with the shaded colours indicating topography in m. The red and green squares show the path of the cyclone based on Joint Typhoon Warning Center (JTWC) best track data, with green colours representing the simulation period considered in the current study. The three letters written in red are the first letters of the three stations, namely Beira, Chimoio and Espungaber, which are plotted at the location of the station. The red rectangle shows the area used for calculations that require area averages.

2.2. Cumulus Schemes

Cumulus schemes represent deep convection, and two main categories are adjustment and mass-flux schemes. Adjustment schemes are designed to relax the atmospheric state towards a moist adiabatic profile when convection is diagnosed, while mass flux schemes incorporate simple models for key processes such as updrafts, downdrafts, entrainment, detrainment and compensating subsidence [23]. The version of WRF used in this study has 15 different cumulus schemes. For this study, we selected five that include the default choice for the tropical suite, and we included both mass-flux and adjustment type schemes. Furthermore, two scale-aware schemes are considered, as these are intended to be more suitable for use in the grey zone [29]. The five schemes are immediately summarised below. The experiments conducted in this study are summarised in Table 1.

- New Tiedtke Scheme [48,50]: The Tiedtke scheme takes a mass flux approach and represents an ensemble of clouds with a bulk plume model. It uses a CAPE closure to determine the strength of the deep and mid-level convection, and has a closure based on surface evaporation for shallow convection.
- New Simplified Arakawa–Schubert (NewSAS) scheme [51]: The NewSAS is a mass flux scheme based on Pan and Wu [52] with revisions made to the entrainment and detrainment formulation following from large-eddy simulation studies. The deep convection was made stronger by increasing the maximum allowable mass flux at the cloud base.

- Multi-Scale Kain–Fritsch (MSKF) scheme [31]: The MSKF is a mass flux scheme that was designed to update the Kain–Fritsch (KF) scheme [53,54], which has no scale dependency and was designed for ∼25 km grids. Scale-dependent parameters that were introduced to KF include the adjustment timescale and the minimum entrainment rate. Updates were also made to the fallout rate and stabilising capacity.
- Grell–Freitas scheme [32]: Grell–Freitas is a mass flux scheme, modified to work across grid sizes from the mesoscale to convective scales. Following a proposal from Arakawa et al. [55], the strength of the parameterized tendency was scaled by a factor $(1 - \sigma)^2$ based on the fractional updraft area σ. As the grid size decreases, the fractional updraft area increases. The scheme places an upper limit on the updraft area by reducing the parameterized cloud radius (or equivalently increasing the initial entrainment rate).
- Betts–Miller–Janjic (BMJ) scheme [56,57]: The BMJ scheme is an update of the Betts–Miller (BM) convective adjustment scheme [58,59]. The deep convection profiles and the relaxation time in BMJ are variable and depend on the cloud efficiency, a nondimensional parameter that characterizes the convective regime.

Table 1. Summary of experimental design.

Model	WRF 4.1.2
Grid length	6 km
Simulation period	00 UTC 13 March to 00UTC 16 March 2019
Forcing global model	Global Forecast System (GFS)
Physics settings Cloud microphysics Planetary boundary layer Short- and long-wave radiation	WRF Single Moment 6 class (WSM6) Yonsei University (YSU) Rapid Radiation Transfer Model (RRTM)
Cumulus schemes (experiments)	New Tiedtke (Tiedtke) New Simplified Arakawa–Schubert (NewSAS) Multi-Scale Kain–Fritsch (MSKF) Grell–Freitas Betts–Miller–Janjic (BMJ) No-convection scheme (NOCP)

2.3. Observations Used

Observed rainfall data from three stations from Mozambique's Instituto Nacional de Meteorologia (INAM) were analysed to indicate the recorded rainfall on the ground during the heavy rainfall event that took place following landfall. The three stations were Beira, Chimoio and Espungaber, whose locations are shown in Figure 1 with the first letter of the station written as a red letter. To study the spatial distribution of rainfall, we use the 30 min interval Integrated Multi-Satellite Retrievals for Global Precipitation Measurement (GPM) (IMERG) rainfall product, calibrated with ground observations [60]. The IMERG product is based on the GPM constellation and is available at a resolution of 0.1°. The data are available through the STORM Precipitation Processing System (PPS) via this URL:https://storm.pps.eosdis.nasa.gov/storm/ (accessed on 23 October 2020). ERA5 reanalyses are the latest climate reanalysis product from ECMWF [61] and these are employed here to study other variables including temperature and winds. ERA5 combines vast amounts of historical observations into global estimates using the Integrated Forecasting System (IFS) and data assimilation systems. The high temporal resolution provided by both IMERG and ERA5 makes it possible for us to study the timing of rainfall. The Joint Typhoon Warning Center (JTWC) best track data were used for the observations of location, minimum sea level pressure and the maximum wind speed of the system.

2.4. Objective Verification

The Mean Error (ME) and Root Mean Square Error (RMSE) were calculated for twenty-four-hour simulated rainfall, with the assessments being made against the IMERG as the observational data. Results of the simulations were interpolated to the IMERG grid using the lterp function in the Grid Analysis and Display System (GrADS) software, by applying bilinear interpolation. In future studies, the conservative method will be applied when interpolating precipitation because of its advantage of using more points to interpolate data [62]. Studies such as [63] have shown that at convective scales, models generally struggle with capturing the precise location of rainfall events, and that simple statistical measures can result in so-called "double penalty" issues. However, simple methods are appropriate here for studying accumulations from a tropical cyclone, for which it is important that a model captures the track of the storm, as well as areas where heavy rainfall is expected. The ME and RMSE [64] are defined as follows:

$$\text{ME} = \bar{F} - \bar{O} \tag{1}$$

$$\text{RMSE} = \sqrt{\frac{1}{N}\Sigma_{i=1}^{n}\left(F_i - O_i\right)^2} \tag{2}$$

where F represents data from one of the simulations, O the observations, i labels grid points and N is the total number of points on the IMERG grid. The statistics are calculated over a rectangle from 24° to 14° S and from 30° to 43° E shown with a red rectangle in Figure 1.

3. Event Description

Tropical cyclone Idai started as a tropical depression from 4 to 8 March 2019 in the Mozambique Channel. The system was associated with wind speeds of about 55 kmh^{-1} with gusts of up to 75 km/h^{-1} and heavy rainfall [14]. The system initially made landfall on the day that it developed, resulting in heavy rainfall in northern parts of Mozambique and southern Malawi. It then moved eastwards back over the warm waters of the Mozambique Channel where it intensified into a tropical cyclone by 11 March. The JTWC best track dataset showed Idai as a tropical storm from 10 March 2019, at 06 UTC, and the system was classified as a tropical cyclone later the same day at 18 UTC. Idai maintained this classification until 15 March 2019, 18 UTC, when the storm became classified as a tropical storm, further downgrading to a tropical depression on 16 March 2019 at 06 UTC. The track of the event using the JTWC data is shown by the red and green squares in Figure 1. On 10 March, the system was over the Mozambique Channel just west of Madagascar, and started moving west on 11 March. Idai made landfall in the Beira area on the evening of 14 March around 22 UTC. The system finally dissipated with the centre of the storm located in eastern Zimbabwe. Idai was therefore long lived, persisting for longer than the mean cyclone lifetime in the SWIO of 7–8 days, as identified by Mavume et al. [7]. NWP models were able to capture the storm track and provide indications that the system would make landfall in the Beira area, with uncertainty in the forecasts being reduced by 12 March [14].

The JTWC best track data timeseries of the maximum wind speed and minimum sea level pressure (SLP) are shown in Figure 2 at six hourly intervals for the 72 h simulation period considered in this study. The highest wind speed observed throughout the period is 115 knots (59 ms^{-1}), while the lowest SLP is 947 hPa. Both the highest wind and lowest SLP were observed on 11 March 2019 at 03 UTC. Another wind peak of 115 knots was observed again on 13 March 2019 18 UTC, with an associated minimum SLP of 948 hPa. The position of the centre of the storm associated with the first peak of the system is 17.3° S and 43° E, just west of Madagascar, and for the second peak, the position is 19.5° S and 38.5° E, also still in the Mozambique Channel before landfall.

Although the system lasted for over 10 days, our study only focused on a three-day period from 00 UTC 13 March to 00 UTC 16 March 2019. This period is indicated by the green squares in Figure 1. This means that our study starts when Idai is already classified as a tropical cyclone and the simulation period includes the time of the second wind

maximum. Our study period also includes landfall which occurred on the evening of 14 March in the Beira area of Mozambique, and it ends after Idai had weakened to a tropical storm in Zimbabwe. Twenty-four-hour rainfall values reported by three INAM weather stations are shown in the second column of Table 2. The Beira station reported 216.9 mm on 15 March 2019, while Chimoio and Espungaber reported 77.7 and 144.3 mm, respectively.
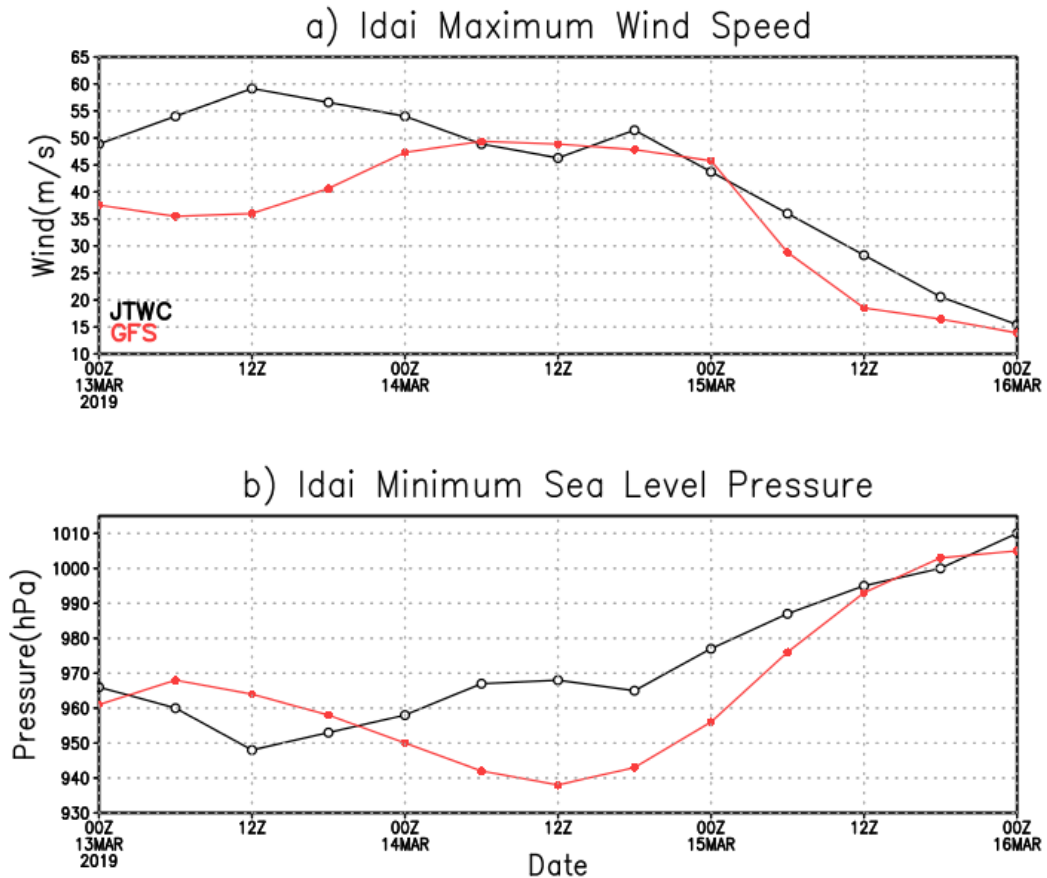
Figure 2. The (**a**) maximum wind speed (m/s) and (**b**) minimum sea level pressure (hPa) during the Idai tropical cyclone based on the Joint Typhoon Warning Center best track data (black line) as well as for GFS data (red line) for the 72 h period considered in this study.

Table 2. The twenty-four-hour rainfall observed in three INAM stations as well as simulated rainfall from the nearest grid point to the station using the six simulations on 15 March 2019.

| City	Obs	BMJ	Grell–Freitas	MSKF	NewSAS	Tiedtke	NOCP
Beira	216.9	159.23	133.47	170.31	168.62	153.36	198.37
Chimoio	77.7	31.67	14.657	13.90	2.72	10.31	20.48
Espungaber	144.3	25.19	34.1324	28.25	21.69	26.64	30.05

4. Results

This section discusses the 3-day simulation results, first separated into the individual days and compared with the ERA5 reanalysis and IMERG. The focus of the discussions is on rainfall and winds as these are the two variables for which extreme values can lead to property damage, injuries and loss of life. The track of the tropical cyclone as well as its minimum SLP were also discussed to assess the intensity of the system.

4.1. Twenty-Four-Hour Total Rainfall

On 13 March 2019, tropical cyclone Idai was over the Mozambique Channel, and the heavy rainfall associated with the storm is shown by ERA5 reanalysis (Figure 3a) and IMERG (Figure 3b). The IMERG rainfall is higher than the ERA5, though the positioning of the heavy rainfall was mostly similar. Both IMERG and ERA5 show some rainfall areas over the south of the Democratic Republic of Congo (DRC), north of Zambia, Malawi, south of Tanzania and north of Mozambique, which are not part of the tropical cyclone. While our primary focus in this study is on Idai, we also compared rainfall amounts and patterns associated with the band of rainfall to its north in order to build more understanding of the behaviour of different cumulus schemes. This rainfall area is more extensive in IMERG than in the ERA5 reanalysis. The performance of IMERG and ERA5 rainfall products was compared over different parts of the globe. Over Austria, both products were found to underestimate rainfall, with an overall result that IMERG outperforms ERA5 in mountainous areas [65]. In the US, Beck et al. [66] found that IMERG outperformed ERA5 in regions dominated by convective storms, while the opposite was found for complex terrain. Dezfuli et al. [67] found the diurnal cycle and rainfall intensity over Africa to be best captured by IMERG compared to other rainfall products. For our study, we used IMERG as the rainfall observation data because of its higher spatial resolution compared to ERA5.
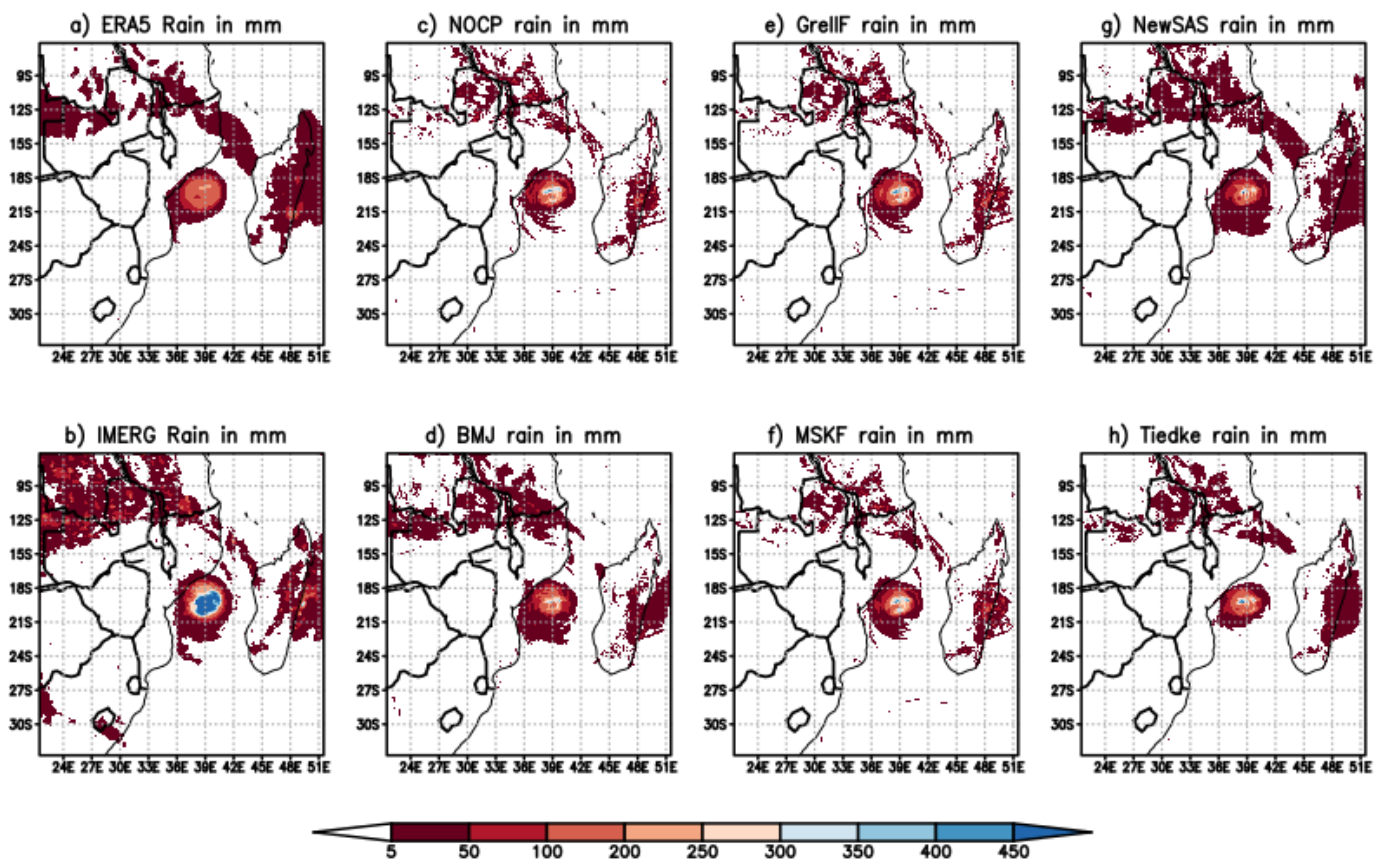
Figure 3. Accumulated rainfall (mm) for 13 March from (**a**) ERA5, (**b**) IMERG, and WRF simulations with (**c**) no-convection scheme, (**d**) the BMJ scheme, (**e**) the Grell–Freitas scheme, (**f**) the MSKF scheme, (**g**) the NewSAS scheme and (**h**) the new Tiedtke scheme.

Figure 3c–h show rainfall simulated with WRF, with the convection scheme switched off (c), and with five different convection schemes (d) to (h). The simulations are plotted on their native grid. The 13 March is day 1 of the simulation and therefore also includes the spin up period. Champion and Hodges [34] found the model spin up period to be between 6 and 12 h, and also that rainfall simulations became unrealistic 48 h after initialisation. On the other hand, Chu et al. [68] concluded that a 60 h spin up produced better results for a flooding event in China, than when shorter spin up time was used. The position of the heavy rainfall associated with Idai is similar across all the simulations, with different patterns in the outer parts of the storm. The area of the cyclone with the heaviest rainfall is smaller in all the simulations when compared to both IMERG and ERA5. The highest rainfall intensities simulated by WRF are comparable with ERA5, but smaller than IMERG. An area of somewhat lighter rainfall on the southern or southeastern flank of the cyclone is most prominent using NewSAS or BMJ but barely perceptible with the new Tiedtke scheme.

There are larger differences in the simulated rainfall patterns over a number of countries including Zambia, Tanzania, Malawi and the DRC. The rainfall pattern is more similar to the ERA5 reanalysis, with less rainfall over the DRC, compared to that in IMERG where the rainfall extends to the northwestern border of the domain in DRC. The simulated rainfall area is smaller and more patchy in the Grell–Freitas and MSKF simulations, while BMJ and NewSAS simulate larger rainfall areas. The ERA5 and IMERG both indicated rainfall amounts of greater than 50 mm over the eastern parts of Madagascar. These larger amounts were captured by Grell–Freitas and MSKF, albeit with smaller areas of rainfall than the other three schemes.

Idai made landfall in the Beira area of Mozambique during the evening of 14 March 2019. Some of the heavy rainfall which was restricted to the ocean on 13 March began to fall over parts of Mozambique, as shown by ERA5 (Figure 4a) and IMERG (Figure 4b). The rainfall band in the northern part of the domain was much reduced, while the rainfall over Madagascar was restricted to the northern half of the country. The simulated rainfall in the centre of the storm was somewhat similar across the different schemes (Figure 4d–h), as well as in the simulation where the convection scheme is switched off (c). However, the storm area does vary in the WRF simulations, and is notably smaller than in the observations without a convection scheme or with the scale-aware schemes MSKF and Grell–Freitas. Over the northern half of Madagascar, NewSAS and Tiedtke simulate rainfall amounts lower than 50 mm. These amounts are similar to ERA5, while IMERG shows higher amounts. The simulation without a convection scheme or those using Grell–Freitas or MSKF produce smaller rainfall elements with some amounts greater than 50 mm.

On 15 March, Idai moved further inland, impacting the eastern parts of Zimbabwe as well as parts of Malawi. The storm was slightly deformed compared to the first two days of simulation, with similar rainfall being indicated by ERA5 (Figure 5a) and IMERG (Figure 5b). The simulated rainfall in the centre of the storm is fairly similar across all of the WRF simulations (Figure 5c–h. The rainfall over Madagascar has now moved to the northwestern parts of the country. Similarly to 14 March, the simulations with no-convection scheme or with Grell–Freitas or MSKF produce many small-scale rainfall elements in this area. BMJ simulates the least rainfall and is similarly patchy, while NewSAS and new Tiedtke produce larger areas of rainfall that extend to the top right border of the domain.
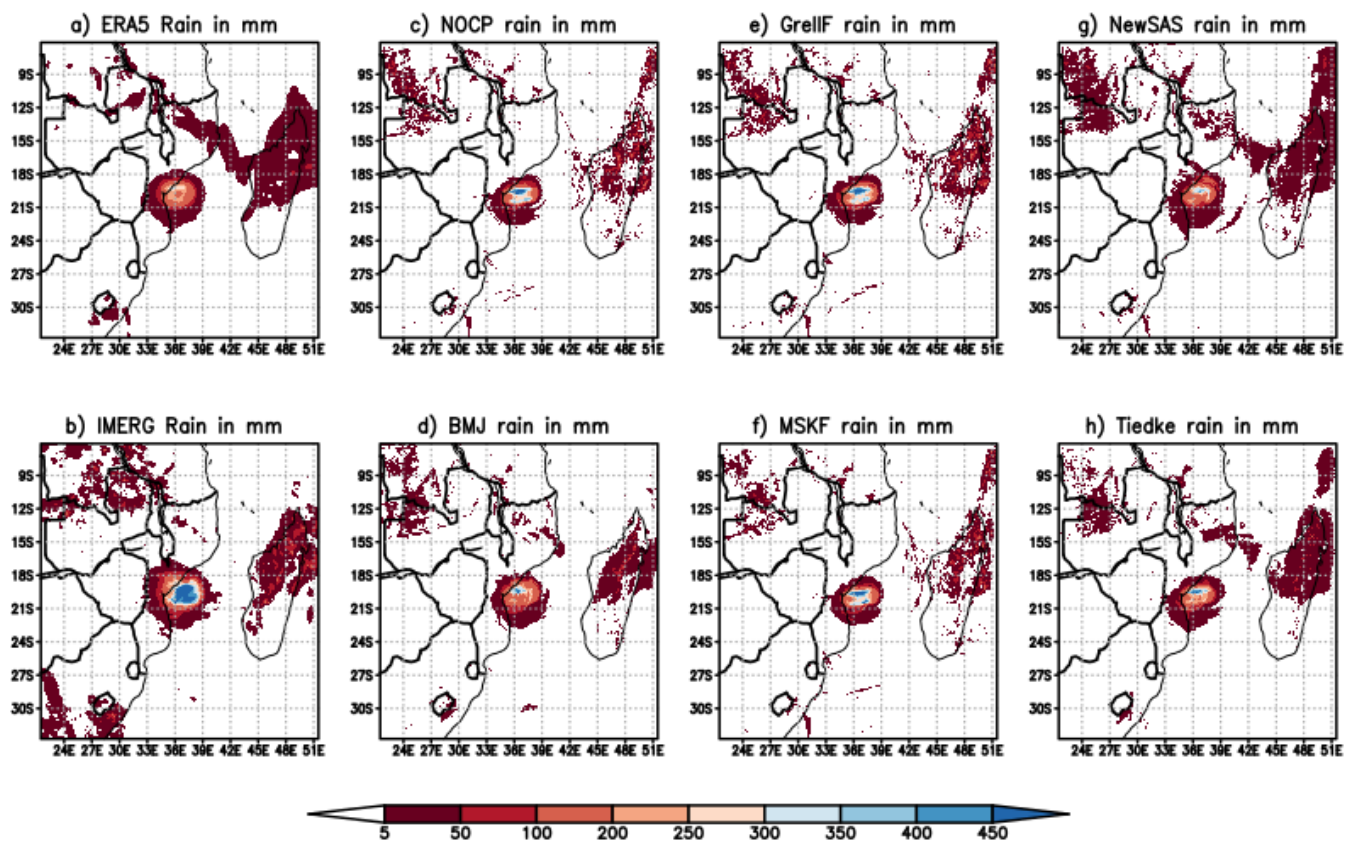
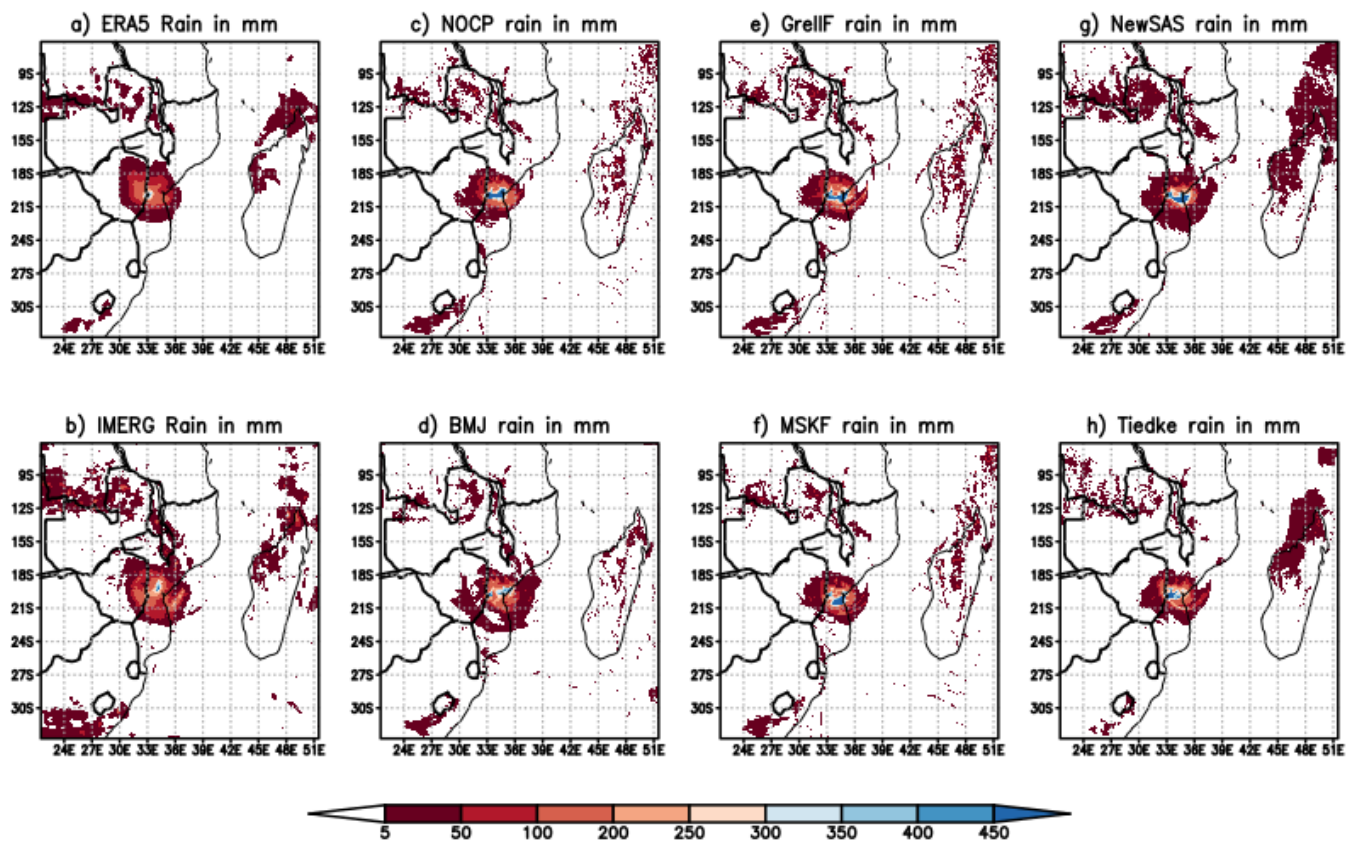**Figure 4.** Same as in Figure 3 but for 14 March.

Figure 5. Same as in Figure 3 but for 15 March.

The bias and RMSE for all six simulations are shown in Table 3, calculated against IMERG data for twenty-four-hour rainfall accumulations. All of the simulations have a negative bias, with a larger magnitude on the first day of simulation, and the least on the third day. This result agrees with the Figure 3 discussion, where it was shown that IMERG indicates a larger rainfall amount associated with the Idai than what is indicated by WRF simulations and ERA5 reanalysis. The rainfall amounts increased in the WRF simulations on the second day with blue colours visible on Figure 4, while for IMERG, the rainfall amount is smaller than for day 1. The IMERG estimated rainfall is more similar in amount to WRF simulations during day 3 (Figure 5) resulting in a smaller bias. The general performance is similar across all the simulations, and there is no particular behaviour associated with different types of convection schemes. The performance of the simulation where the convection scheme is switched off is also similar to simulations with the different convection schemes.

Table 3. The Mean Error and Root Mean Square Error (mm) for the three days of the case study, for WRF simulations with no-convection scheme and with five convection schemes calculated for the red rectangle in Figure 1.

	13 March 2019					
	BMJ	**Grell–Freitas**	**MSKF**	**NewSAS**	**Tiedtke**	**NOCP**
Bias	−20.74	−20.22	−20.42	−21.27	−21.79	−21.03
RMSE	77.36	73.42	72.14	80.45	76.98	74.27
	14 March 2019					
	BMJ	**Grell–Freitas**	**MSKF**	**NewSAS**	**Tiedtke**	**NOCP**
Bias	−18.65	−17.67	−18.36	−19.27	−19.65	−18.93
RMSE	62.93	58.16	62.74	66.76	66.64	61.76
	15 March 2019					
	BMJ	**Grell–Freitas**	**MSKF**	**NewSAS**	**Tiedtke**	**NOCP**
Bias	−4.58	−2.47	−3.77	−3.87	−4.4	−3.9
RMSE	39.06	53.67	59.4	52.58	43.37	47.48

4.2. Resolved Versus Convective and Hourly Rainfall

To further study the differences in simulations made with different schemes, in this subsection, we separate the total rainfall into the convective (subgrid) and resolved parts, as shown in Figure 6. The left and right columns show convective and resolved rainfall for all five schemes summed over all simulated days. With the assumption that the spin up period is up to 12 h [34] the first 12 h of the simulation are discarded from this plot. We do not show the NOCP simulation in this figure because all of the rainfall shown in Figures 3–5 is resolved by definition when the convection scheme is switched off.

Figure 6 shows behaviour related to convection scheme type. The two scale aware schemes (i.e., Grell–Freitas in Figure 6c and MSKF in Figure 6e) are intended to limit the strength of parameterized convection at resolutions where the convective motions can be partially captured by the model dynamics. A grid length of 6 km lies within the deep convection grey zone [29], and approaches convective scales [38] where some of the strongest deep convection might be captured by explicit motions. These methods do indeed result in less convective rainfall in the vicinity of Idai, over Madagascar, and over those countries affected by the band to the north on 13 March. The model dynamics are able to compensate, in the sense that the two schemes produce the most resolved rainfall, this being particularly apparent over Madagascar and the northern parts of the domain. The behaviour of the adjustment scheme BMJ is broadly similar to that of the other mass flux schemes, NewSAS and new Tiedtke. Using these schemes, the rainfall at the heart of the tropical cyclone is mainly associated with the resolved motions, but there is also a

substantial contribution from convection schemes, reaching over 50 mm. The convective rainfall also covers a broader area than the resolved part. The rainfall over Madagascar and within the northern band is dominated by the convection scheme in these cases.
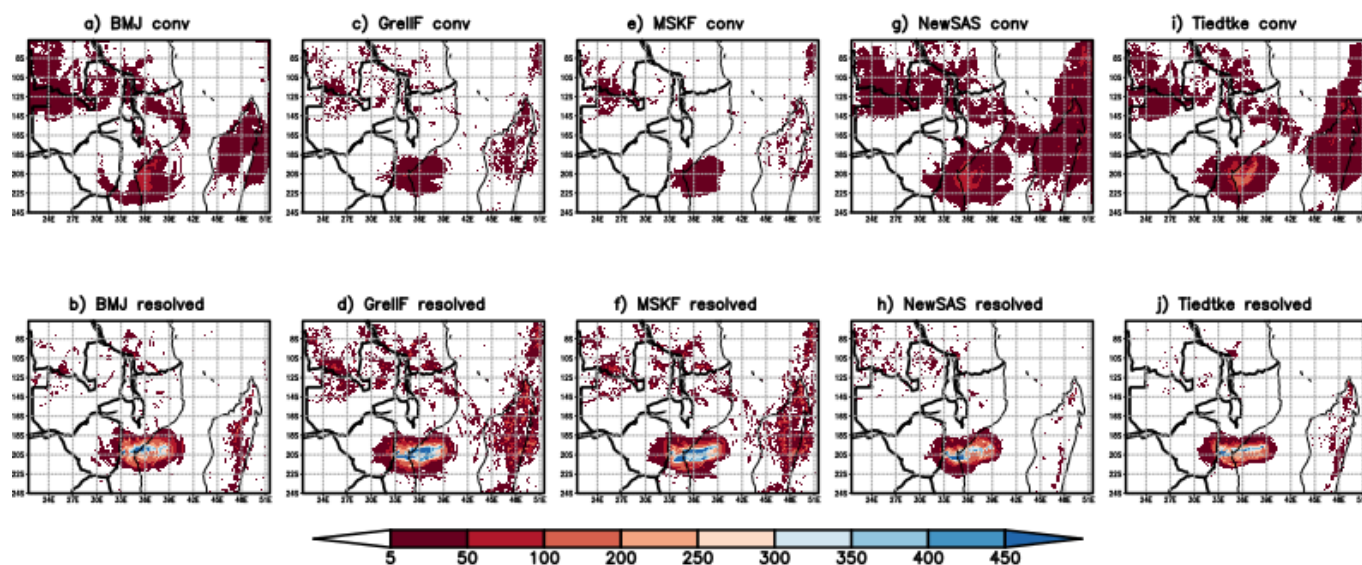
Figure 6. Accumulated rainfall (mm) for 13–15 March from simulations using (**a**,**b**) the BMJ scheme, (**c**,**d**) the Grell–Freitas scheme, (**e**,**f**) the MSKF scheme, (**g**,**h**) the NewSAS scheme and (**i**,**j**) the new Tiedtke scheme. The convective and resolved components of the model rainfall are presented in the left (panels (**a**,**c**,**e**,**g**,**i**)) and right (panels (**b**,**d**,**f**,**h**,**j**)) columns, respectively.

In Figure 7, we consider the rainfall on an hourly timescale, in terms of the maximum rainfall, the area average total and convective rainfall and the contribution from the convection scheme. The area considered is 24° to 14° S and from 30° to 43° E shown in Figure 1. The ERA5 maximum rainfall is lower than for all of the WRF simulations and IMERG throughout the 72 h period (Figure 7a). IMERG maximum rainfall is higher than WRF simulations in the first day and a half but mostly lower in the last 24 h. When comparing the maximum rainfall, it should be noted that the ERA5, IMERG and WRF simulations have different resolutions. The timing of the WRF simulated maximum rainfall is similar across all simulations, with the highest rainfall in the last 24 h. Tiedtke simulated a higher peak than in the other simulations during the early hours of 15 March, which is close to one of the IMERG peaks. The Grell–Freitas scheme also simulated a peak a little later that morning, somewhat higher than in IMERG. The evolution of area average rainfall is very similar across all of the simulations and the ERA5 reanalysis, but IMERG does indicate higher amounts (Figure 7b). The area average hourly convective rainfall confirms that the activity from the convection scheme is suppressed by the scale-aware MSKF and Grell–Freitas schemes (Figure 7c). The NewSAS and Tiedtke simulate the highest convective rainfall amounts during most of the 72 h period, and given the very similar total area averages in Figure 7b, therefore also the lowest resolved rainfall amounts. The BMJ scheme simulates two peaks in convective rainfall (dips in the resolved rainfall), towards the end of day on 13 March and another in the early hours of 14 March. It varies from producing the lowest to the highest convective rainfall out of the five schemes.
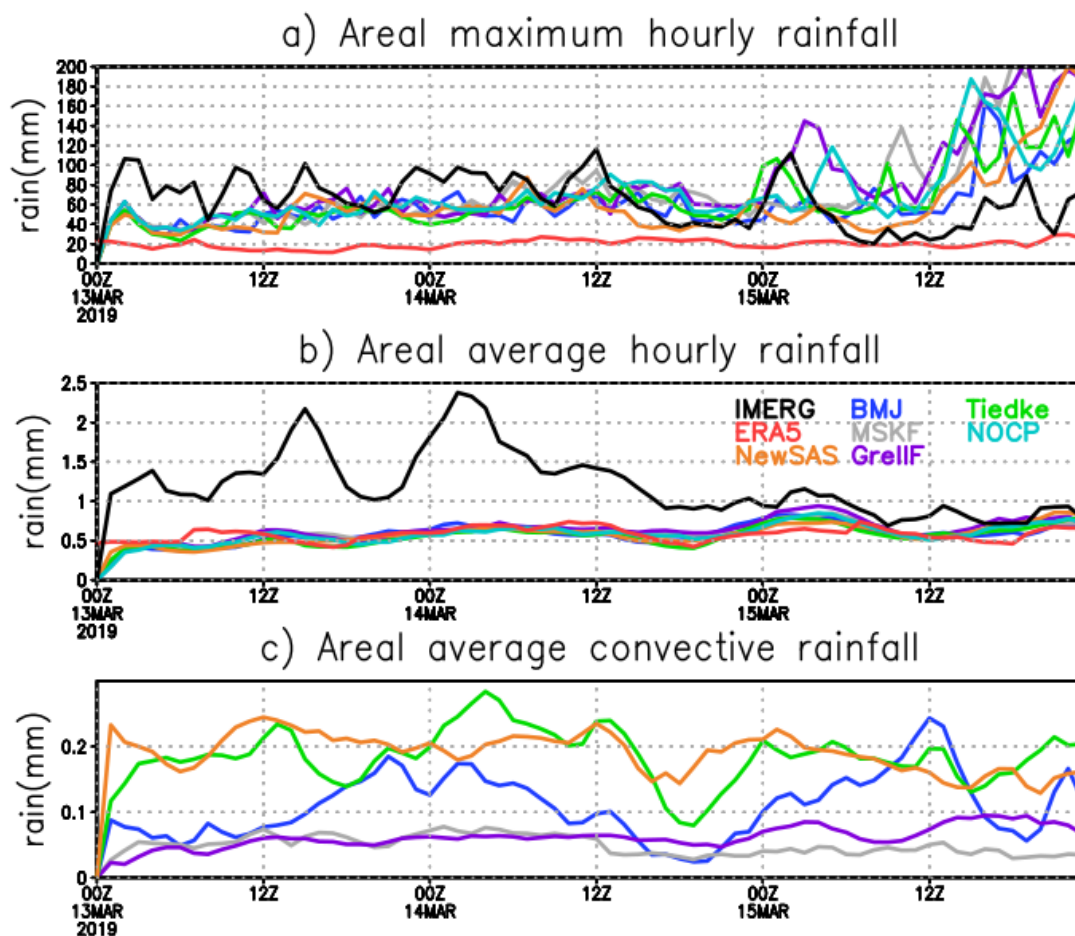
Figure 7. (**a**) The maximum rainfall over the model domain, (**b**) the area average hourly rainfall and (**c**) the area average convective rainfall. The results are shown for IMERG (black) and ERA5 (red) in (**a**,**b**) as well as from WRF simulations using the NewSAS scheme (orange), the BMJ scheme (blue), the MSKF scheme (grey), the Grell–Freitas scheme (purple), the new Tiedtke scheme (green) and the simulation without a cumulus scheme (cyan).

4.3. Wind and Minimum Sea Level Pressure

Another key variable in tropical cyclones is the wind, with strong winds being responsible for a major part of the damage caused by these systems. We examined hourly 10 m winds in the GFS, JTWC best track data and all of the WRF simulations in Figure 8. The second peak of the storm is within the simulation period considered in this study. The peak is shown at 12h00 UTC, associated with higher maximum wind speed and lower minimum SLP according to the JTWC best track. The GFS did not capture this peak. A smaller peak was observed at 18h00 UTC in the JTWC data. The GFS simulated a peak steeper than in JTWC at 12h00 UTC on 14 March according to minimum SLP. However, the maximum winds did not exceed the peak of JTWC.

WRF simulations are generally similar for the first 6 h of simulation. The highest maximum winds are found to be simulated by the two scale aware schemes, MSKF and Grell–Freitas, and by the no-convection scheme simulation. The maximum wind speeds decreased significantly in the first twelve hours of the third day, but the NewSAS simulation lagged behind the others. Figure 8b shows the minimum SLP, and the scale aware schemes simulate the lowest cyclone pressure, alongside the simulation without a cumulus scheme. A lag in the decay of the system is again apparent using the newSAS scheme. The timing of the WRF simulated peak of the storm in the simulation period was modulated by the GFS. Similar to the GFS, WRF does not capture the peak observed at 12h00 UTC on 13 March 2019. The conventional schemes reduce the GFS deep which occurs at a wrong time more

than scale aware ones. The intensity of the storm as simulated by the conventional schemes is found to be generally lower compared to Grell–Freitas and MSKF. Ma and Tan [69] compared the Kain–Fritsch, Betts–Miller and Grell scheme using a grid length of 15 km, and also found the intensity of three tropical cyclones to be underestimated by all three schemes compared to JTWC data.
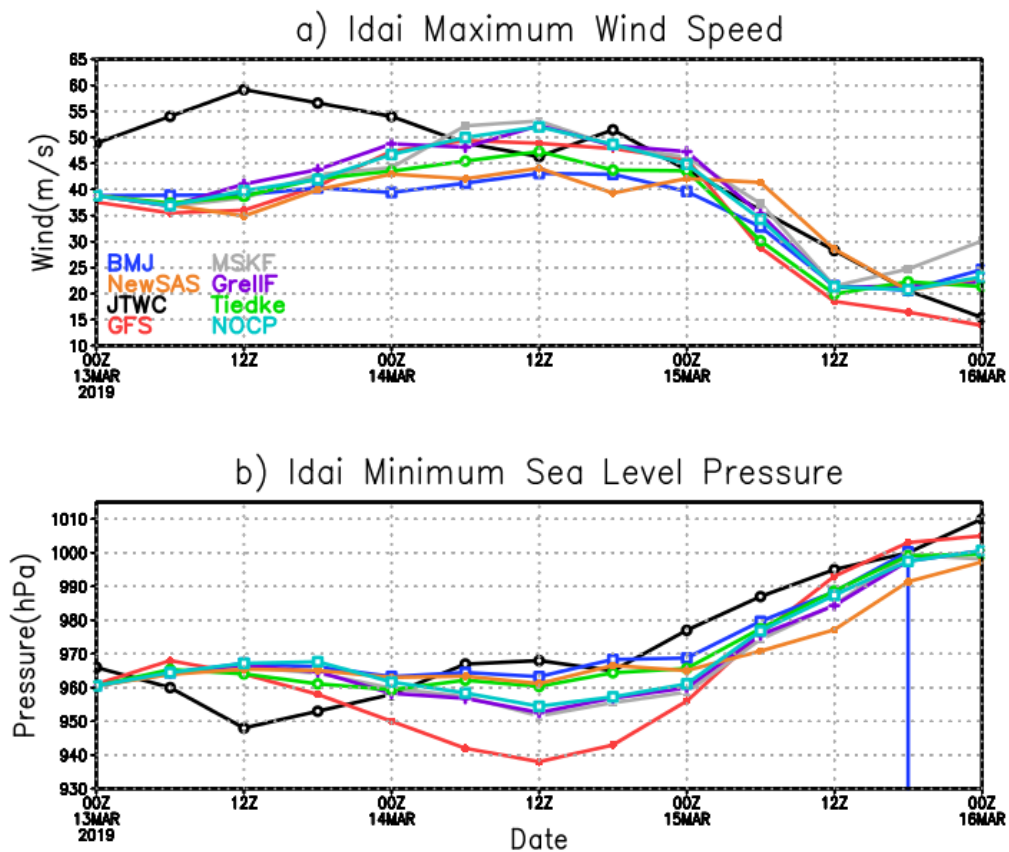

Figure 8. Six hourly (**a**) maximum wind speed and (**b**) minimum SLP as simulated by WRF and GFS and from the JTWC best track data.

4.4. Storm Location

We complete our analysis by considering the location and track of the cyclone. The assessment is based on a comparison of the location data reported by JTWC and the minimum negative vorticity location in each of the simulations. The lowest values of negative vorticity (representing cyclonic flow in Southern Hemisphere) are found in the scale aware schemes, consistent with the intensity of the cyclone as measured from the minimum SLP. Figure 9 shows the simulated position of the minimum vorticity centre at six-hourly intervals. The plot also shows the location based on JTWC data and GFS using the GFDL vortex tracker.

According to the WMO report [14] on tropical cyclone Idai, different models indicated that Idai would make landfall in the Beira area on 14 March with a two-day lead time. All of the simulated storm tracks captured this well and are generally aligned with the observed track. There are some differences in the position of the storm especially after landfall, and BMJ and Tiedtke simulations moved the storm too far to the north and south, respectively. The MSKF and Grell–Freitas scheme also positioned the storm slightly north of the observations at this time. The observed track propagates more quickly than in the simulations, especially in comparison with the NewSAS simulation. Idai crosses into Zimbabwe at the end of the period, but only the NOCP simulation captures this effect. The GFS also missed the crossing by moving the storm towards the north of Mozambique.
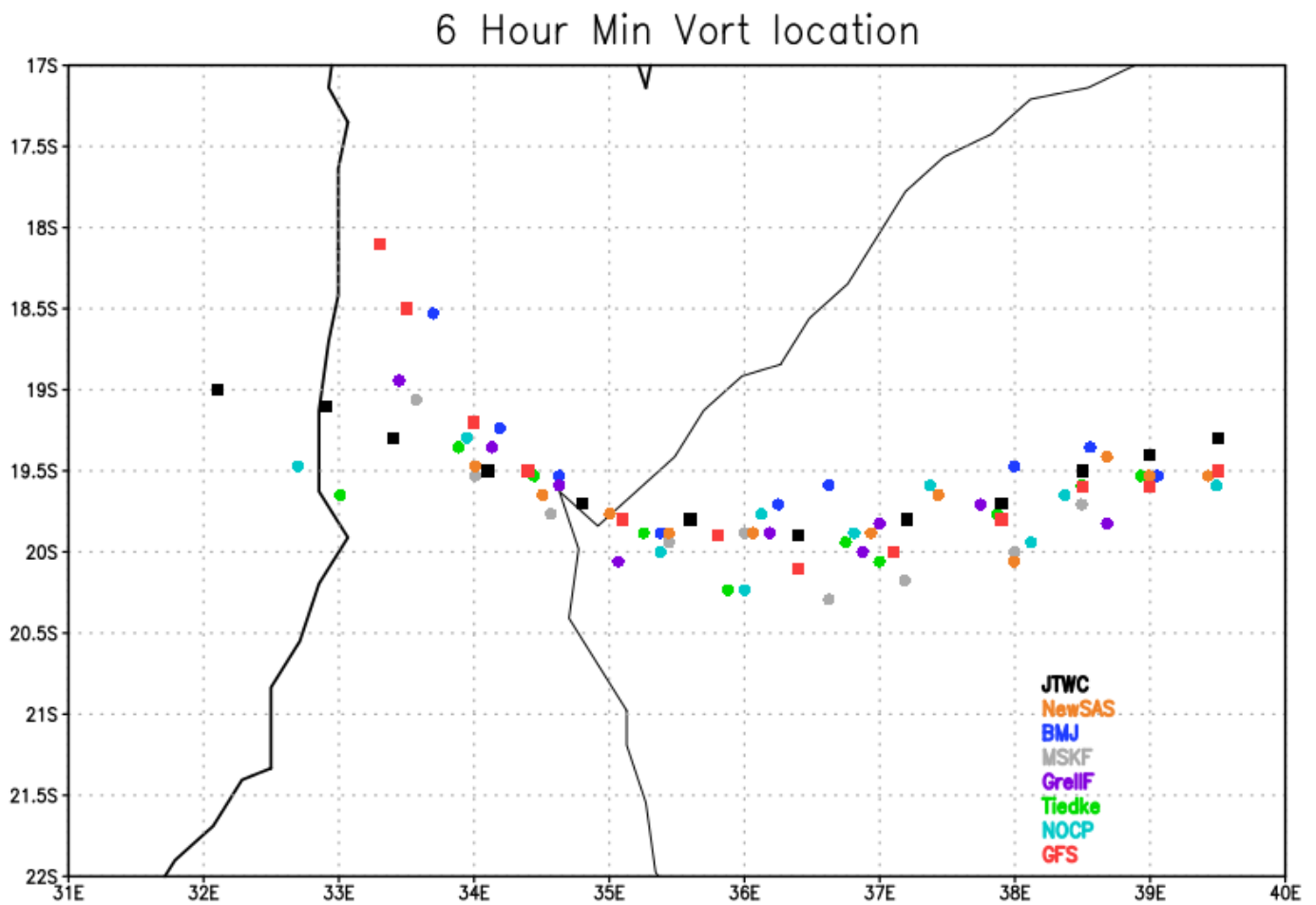
Figure 9. The simulated location of tropical cyclone Idai using 6 h data that match the JTWC time interval for the six experiment, GFS as well as JTWC reported location.

5. Summary and Conclusions

In this study, we investigated the sensitivity of simulations of the tropical cyclone Idai to different choices of cumulus schemes. Simulations are made with the WRF model for a 72 h period starting on 00UTC 13 March. The actual cyclone, together with the depressions associated with it, lasted for over 10 days; however, our study focuses on a period of 72 h when some of its strongest impacts were felt due to the landfall in the Beira area of Mozambique on the evening of 14 March. The selected schemes for this study are Tiedtke (which is the WRF default choice for its tropical suite), Betts–Miller–Janjic, NewSAS, Grell–Freitas and Multi-Scale Kain–Fritsch. We also considered a simulation in which no cumulus scheme is activated. Shepherd and Walsh [70] found that the cumulus scheme has a larger impact on the tracks than shallow convection, initialisation time and model domain size.

The total simulated rainfall and the broad scale rainfall patterns in all of these cases are similar (Sections 4.1 and 4.3) but the rainfall is lower than that in IMERG. This is perhaps partly a consequence of spin up effects: the bias calculations show a larger negative rainfall bias on the first day of simulation, which reduces over the three-day period (Section 4.1). The spin up period was found to be 24 h by Bonekamp et al. [71], while Champion and Hodges [34] found the spin period to be between 6 and 12 h, and that this was associated with some unrealistic precipitation intensities. In our study, we found a spike in wind speed for all of the experiments two hours into the simulation, which stabilised soon after.

We partitioned the simulated rainfall into the component associated with resolved motions and that produced by the convection scheme. While the total rainfall in the domain

is similar in all simulations, its partition considerably varies according to the cumulus treatment chosen (Section 4.2). The mass flux schemes without explicit scale awareness (Tiedtke and NewSAS) have roughly similar contributions from the two components when averaged over the model domain. The mass flux schemes with scale awareness (MSKF and Grell–Freitas) reduce the rainfall produced by the cumulus scheme by around a quarter and thus allow the model dynamics to resolve most of the rainfall. The partitioning varied over time using the adjustment scheme BMJ between the levels associated with the different mass flux schemes. By definition, a simulation without a cumulus scheme has zero convective rainfall.

Several aspects of the differences in the simulation results can be well understood in terms of how the total rainfall is partitioned. Away from the tropical cyclone, in the northern part of the domain, as well as over the eastern parts of Madagascar, there are areas of rainfall that are more different amongst the different schemes. The simulations with more rainfall from the cumulus scheme produce smoother patterns of daily rainfall, while those with little or no convective rainfall produce more patchy, smaller-scale, broken areas of rain which include some larger peak values (Section 4.1). Over Madagascar, IMERG indicates daily rainfall amounts greater than 50 mm, and the only schemes to capture this amount are MSKF and Grell–Freitas. Simulations with little to no convective rainfall also produced a more intense tropical cyclone (Section 4.3), as indicated by the higher maximum wind speed and lower minimum SLP. The timing of the peak is found to be informed by the global model providing lateral boundary conditions, indicating a need to use global models with good skill when running dynamical downscalers. Previous other studies have shown that switching off the convection schemes results in higher rainfall intensity (e.g., [33,34]).

A number of previous studies have also compared the performance of different convection schemes with different conclusions. For example, using resolutions of approximately 110, 35 and 25 km, Kanase et al. [72] found that BMJ outperformed two versions of the Simplified Arakawa–Schubert (SAS) schemes with both convective rainfall and intensity of storms in the north Indian Ocean when simulating three tropical cyclones. On the other hand, Reddy et al. [73] found that BMJ produced lower intensity compared to the Kain–Fritsch and Grell–Devenyi ensemble schemes when simulating tropical cyclone Jal, also in north Indian Ocean. Fahad and Tanvir [74] found that not using the convection scheme resulted in less accurate simulations regarding sea level pressure, total precipitation as well as the track of the system. They found the mass flux type schemes (Kain–Fristch and Grell) produced better results than BMJ, with Kain–Fritsch performing the best overall. Biswas et al. [75] compared the SAS, NewSAS, Kain–Fritsch and Tiedtke schemes when simulating a number of tropical cyclones and found the tracks and storm structure to be superior with SAS compared to the other schemes. For our study, overall, we can conclude that scale-aware schemes allow the model dynamics to do most of the work and simulate higher intensity than conventional ones in the grey zone. None of the schemes can solve challenges with the driving data indicating a need to force limited area models in operational forecasting with better performing global models.

Appendix A

The WRF namelist is below showing options used. cu_physics was changed to match different convection schemes, while 11 other parameters remained the same.

Table A1. This is a table caption. Tables should be placed in the main text near to the first time they are cited.

Parameter Name	Parameter Selection
run_days	=0,
run_hours	=72,
run_minutes	=0,
run_seconds	=0,
start_year	=2019,
start_month	=03,
start_day	=13,
start_hour	=00,
end_year	=2019,
end_month	=03,
end_day	=16,
end_hour	=00,
y interval_seconds	=10,800
input_from_file	=.true.,
history_interval	=60,
frames_per_outfile	=1,
restart	=.false.,
restart_interval	=1440,
time_step	=36,
time_step_fract_num	=0,
time_step_fract_den	=1,
max_dom	=1,
e_we	=484,
e_sn	=460,
e_vert	=33,
p_top_requested	=5000,
num_metgrid_levels	=32,
num_metgrid_soil_levels	=4,

Table A1. *Cont.*

Parameter Name	Parameter Selection
dx	=6000,
dy	=6000,
grid_id	=1,
parent_id	=0,
i_parent_start	=1,
j_parent_start	=1,
parent_grid_ratio	=1,
parent_time_step_ratio	=1,
feedback	=1,
smooth_option	=0
physics_suite	='TROPICAL'
mp_physics	=−1,
cu_physics	=2,
ra_lw_physics	=−1,
ra_sw_physics	=−1,
bl_pbl_physics	=−1,
sf_sfclay_physics	=−1,
sf_surface_physics	=−1,
radt	=30,
bldt	=0,
cudt	=5,
icloud	=1,
num_land_cat	=21,
sf_urban_physics	=0,

References

1. Houze, R.A.J. *Cloud Dynamics*; Academic Press: Cambridge, MA, USA, 1994; p. 573.
2. Knight, D.; Davis, R. Contribution of tropical cyclones to extreme rainfall in the Southeastern United States. *J. Geophys. Res.* **2009**, *114*. [CrossRef]
3. Pillay, M.; Fitchett, J. Southern Hemisphere Tropical Cyclones: A Critical Analysis of Regional Characteristics. *Int. J. Climatol.* **2020**, *41*. [CrossRef]
4. Mendelsohn, R.; Molua, E.; Akamin, A. Economic vulnerability to tropical storms on the southeastern coast of Africa. *JàMbá J. Disaster Risk Stud.* **2020**, *12*, 2072–2845. [CrossRef]
5. Chikoore, H.; Vermeulen, J.; Jury, M. Tropical cyclones in the Mozambique Channel: January–March 2012. *Nat. Hazards* **2015**, *77*. [CrossRef]
6. Davis-Reddy, C.; Vincent, K. Climate Risk and Vulnerability: A Handbook for Southern Africa (Second Edition) CSIR. 2017. Available online: https://www.csir.co.za/sites/default/files/Documents/SADC%20Handbook_Second%20Edition_full%20report.pdf (accessed on 10 May 2021).
7. Mavume, A.; Rydberg, L.; Rouault, M.; Lutjeharms, J. Climatology and Landfall of Tropical Cyclones in the South-West Indian Ocean. *West. Indian Ocean. J. Mar. Sci.* **2010**, *8*. [CrossRef]
8. Reason, C.J.C.; Keibel, A. Tropical Cyclone Eline and Its Unusual Penetration and Impacts over the Southern African Mainland. *Weather Forecast.* **2004**, *19*, 789–805. [CrossRef]
9. Moses, O.; Ramotonto, S. Assessing forecasting models on prediction of the tropical cyclone Dineo and the associated rainfall over Botswana. *Weather Clim. Extrem.* **2018**, *21*, 102–109. [CrossRef]
10. Mhlanga, C.; Muzingili, T.; Mpambela, M. Natural disasters in Zimbabwe: The primer for social work intervention. *Afr. J. Soc. Work.* **2019**, *9*, 46–54.
11. Reunion, M.F.L. Past and Current Hurricane System. Available online: http://www.meteofrance.re/cyclone/saisons-passees (accessed on 30 April 2021).
12. Malherbe, J.; Engelbrecht, F.; Landman, W. Projected changes in tropical cyclone climatology and landfall in the Southwest Indian Ocean region under enhanced anthropogenic forcing. *Clim. Dyn.* **2013**, *40*. [CrossRef]
13. Yu, P.; Johannessen, J.A.; Yan, X.H.; Geng, X.; Zhong, X.; Zhu, L. A Study of the Intensity of Tropical Cyclone Idai Using Dual-Polarization Sentinel-1 Data. *Remote Sens.* **2019**, *11*, 2837. [CrossRef]

14. Wolrd Meteorological Organization. *Reducing Vulnerability to Extreme Hydro-Meteorological Hazards in Mozambique after Cyclone IDAI: WMO Mission Report Following Tropical Cyclone IDAI*; WMO: Geneva, Switzerland, 2019; p. 64.

15. Mongo, E.; Cambaza, E.; Nhambire, R.; Singo, J.; Machava, E. Outbreak of Cholera Due to Cyclone Idai in Central Mozambique. In *Evaluation of Health Services*; IntechOpen: London, UK, 2020; pp. 1–8. [CrossRef]

16. Zimba, S.K.; Houane, M.J.; Chikova, A.M. Impact of Tropical Cyclone Idai on the Southern African Electric Power Grid. In Proceedings of the 2020 IEEE PES/IAS PowerAfrica, Nairobi, Kenya, 25–28 August 2020; pp. 1–5. [CrossRef]

17. Charrua, A.B.; Padmanaban, R.; Cabral, P.; Bandeira, S.; Romeiras, M.M. Impacts of the Tropical Cyclone Idai in Mozambique: A Multi-Temporal Landsat Satellite Imagery Analysis. *Remote Sens.* **2021**, *13*, 201. [CrossRef]

18. Frieden, M. *The Aftermath of Cyclone Idai—Building Bridges Where We Can*; BMJ Publishing Group: London, UK, 2019.

19. Chari, F.; Ngcamu, B.; Novukela, C. Supply chain risks in humanitarian relief operations: A case of Cyclone Idai relief efforts in Zimbabwe. *J. Humanit. Logist. Supply Chain. Manag.* **2020**, *10*, 320–361. [CrossRef]

20. Suarez, P. *Linking Climate Knowledge and Decisions: Humanitarian Challenges*; Boston University: Boston, MA, USA, 2009.

21. Bauer, P.; Thorpe, A.; Brunet, G. The quiet revolution of numerical weather prediction. *Nature* **2015**, *525*, 47–55. [CrossRef] [PubMed]

22. Dyson, L.; Van Heerden, J. The heavy rainfall and floods over the northeastern interior of South Africa during February 2000. *S. Afr. J. Sci.* **2001**, *97*, 80–86.

23. Stensrud, D. Parametrization schemes. Keys to understanding numerical weather Prediction models. Reprint of the 2007 hardback ed. In *Parameterization Schemes: Keys to Understanding Numerical Weather Prediction Models*; Cambridge University Press: Cambridge, UK, 2007; p. 480. [CrossRef]

24. Villafuerte, M., II; Lambrento, J.; Hodges, K.; Cruz, F.; Cinco, T.; Narisma, G. Sensitivity of tropical cyclones to convective parameterization schemes in RegCM4. *Clim. Dyn.* **2021**, *56*, 1–18. [CrossRef]

25. Fuentes Franco, R.; Giorgi, F.; Coppola, E.; Zimmermann, K. Sensitivity of tropical cyclones to resolution, convection scheme and ocean flux parameterization over Eastern Tropical Pacific and Tropical North Atlantic Oceans in the RegCM4 model. *Clim. Dyn.* **2017**, *49*. [CrossRef]

26. Lim, Y.K.; Schubert, S.D.; Reale, O.; Lee, M.I.; Molod, A.M.; Suarez, M.J. Sensitivity of Tropical Cyclones to Parameterized Convection in the NASA GEOS-5 Model. *J. Clim.* **2015**, *28*, 551–573. [CrossRef]

27. Radhakrishnan, C.; Balaji, C. Sensitivity of tropical cyclone Jal simulations to physics parameterizations. *J. Earth Syst. Sci.* **2012**, *121*. [CrossRef]

28. Davis, C. Resolving Tropical Cyclone Intensity in Models. *Geophys. Res. Lett.* **2018**, *45*. [CrossRef]

29. Steeneveld, G.J.; Peerlings, E. Mesoscale Model Simulation of a Severe Summer Thunderstorm in The Netherlands: Performance and Uncertainty Assessment for Parameterised and Resolved Convection. *Atmosphere* **2020**, *11*, 811. [CrossRef]

30. Honnert, R.; Efstathiou, G.A.; Beare, R.J.; Ito, J.; Lock, A.; Neggers, R.; Plant, R.S.; Shin, H.H.; Tomassini, L.; Zhou, B. The Atmospheric Boundary Layer and the "Gray Zone" of Turbulence: A Critical Review. *J. Geophys. Res. Atmos.* **2020**, *125*, e2019JD030317. [CrossRef]

31. Zheng, Y.; Alpaty, K.; Herwehe, J.A.; Del Genio, A.D.; Niyogi, D. Improving high-resolution weather forecasts using the Weather Research and Forecasting (WRF) model with an updated Kain-Fritsch scheme. *Mon. Weather Rev.* **2016**, *144*, 833–860. [CrossRef]

32. Grell, G.A.; Freitas, S.R. A scale and aerosol aware stochastic convective parameterization for weather and air quality modeling. *Atmos. Chem. Phys.* **2014**, *14*, 5233–5250. [CrossRef]

33. Somses, S.; Bopape, M.J.M.; Ndarana, T.; Fridlind, A.; Matsui, T.; Phaduli, E.; Limbo, A.; Maikhudumu, S.; Maisha, R.; Rakate, E. Convection parametrization and multi-nesting dependence of a heavy rainfall event over Namibia with Weather Research and Forecasting (WRF) model. *Climate* **2020**, *8*, 112. [CrossRef]

34. Champion, A.; Hodges, K. Importance of resolution and model configuration when downscaling extreme precipitation. *Tellus A* **2014**, *66*. [CrossRef]

35. Skamarock, W.C.; Klemp, J.B.; Dudhia, J.; Gill, D.O.; Liu, Z.; Berner, J.; Huang, X.Y. *A Description of the Advanced Research WRF Model Version 4 (No. NCAR/TN-556+STR)*; National Center for Atmospheric Research: Boulder, CO, USA, 2008.

36. Powers, J.G.; Klemp, J.B.; Skamarock, W.C.; Davis, C.A.; Dudhia, J.; Gill, D.O.; Coen, J.L.; Gochis, D.J.; Ahmadov, R.; Peckham, S.E.; et al. The Weather Research and Forecasting Model: Overview, System Efforts, and Future Directions. *Bull. Am. Meteorol. Soc.* **2017**, *98*, 1717–1737. [CrossRef]

37. Bopape, M.M.; Sithole, H.; Motshegwa, T.; Rakate, E.; Engelbrecht, F.; Morgan, A.; Ndimeni, L.; Botai, O.J. A Regional Project in Support of the SADC Cyber-Infrastructure Framework Implementation: Weather and Climate. *Data Sci. J.* **2019**, *18*, 34. [CrossRef]

38. Clark, P.; Roberts, N.; Lean, H.; Ballard, S.; Charlton-Perez, C. Convection-permitting models: A step-change in rainfall forecasting. *Meteorol. Appl.* **2016**, *23*. [CrossRef]

39. Weisman, M.; Skamarock, W.; Klemp, J. The Resolution Dependence of Explicitly Modeled Convective Systems. *Mon. Weather Rev.* **1997**, *125*. [CrossRef]

40. Roberts, N. Assessing the spatial and temporal variation in the skill of precipitation forecasts from an NWP model. *Meteorol. Appl.* **2008**, *15*, 163–169. [CrossRef]

41. Bryan, G.; Wyngaard, J.; Fritsch, J. Resolution Requirements for the Simulation of Deep Moist Convection. *Mon. Weather Rev.* **2003**, *131*. [CrossRef]

42. Sela, J. Implementation of the sigma pressure hybrid coordinate into GFS. *NCEP Off. Note* **2009**, *461*, 1–25.

43. Wang, W. *WRF: More Runtime Options*; WRF Tutorial, UNSW: Sydney, Australia, 2017; p. 46.
44. Sun, B.Y.; Bi, X. Validation for a tropical belt version of WRF: Sensitivity tests on radiation and cumulus convection parameterizations. *Atmos. Ocean. Sci. Lett.* **2019**, *12*, 192–200. [CrossRef]
45. Iacono, M.; Delamere, J.; Mlawer, E.; Shepard, M.; Clough, S.; Collins, W. Radiative Forcing by Long-Lived Greenhouse Gases: Calculations with the AER Radiative Transfer Models. *J. Geophys. Res.* **2008**, *113*. [CrossRef]
46. Hong, S.Y.; Kim, J.H.; Lim, J.O.; Dudhia, J. The WRF single moment microphysics scheme (WSM). *J. Korean Meteorol. Soc.* **2006**, *42*, 129–151.
47. Hong, S.Y.; Noh, Y.; Dudhia, J. A New Vertical Diffusion Package with an Explicit Treatment of Entrainment Processes. *Mon. Weather Rev.* **2006**, *134*, 2318–2341. [CrossRef]
48. Zhang, C.; Wang, Y.; Hamilton, K. Improved Representation of Boundary Layer Clouds over the Southeast Pacific in ARW-WRF Using a Modified Tiedtke Cumulus Parameterization Scheme. *Mon. Weather Rev.* **2011**, *139*, 3489–3513. [CrossRef]
49. Zhang, S.; Matsui, T.; Cheung, S.; Zupanski, M.; Peters-Lidard, C. Impact of Assimilated Precipitation-Sensitive Radiances on the NU-WRF Simulation of the West African Monsoon. *Mon. Weather Rev.* **2017**, *145*. [CrossRef]
50. Tiedtke, M. A Comprehensive Mass Flux Scheme For Cumulus Parameterization In Large-Scale Models. *Mon. Weather Rev.* **1989**, *117*. [CrossRef]
51. Han, J.; Pan, H.L. Revision of Convection and Vertical Diffusion Schemes in the NCEP Global Forecast System. *Weather Forecast.* **2011**, *26*, 520–533. [CrossRef]
52. Pan, H.L.; Wu, W.S. *Implementing a Mass Flux Convective Parameterization Package for the NMC Medium-Range Forecast Model*; NMC Office Note 409; National Centers for Environmental Prediction: Silver Spring, MD, USA, 1995; 40p.
53. Kain, J.S.; Fritsch, J.M. A one-dimensional entraining/detraining plume model and its application in convective parameterization. *J. Atmos. Sci.* **1990**, *47*, 2784–2802. [CrossRef]
54. Kain, J.S. The Kain–Fritsch convective parameterization: An update. *J. Appl. Meteorol.* **2004**, *43*, 170–181. [CrossRef]
55. Arakawa, A.; Jung, J.H.; Wu, C.M. Toward unification of the multiscale modeling of the atmosphere. *Atmos. Chem. Phys.* **2011**, *11*, 3731–3742. [CrossRef]
56. Janjić, Z.I. The Step-Mountain Eta Coordinate Model: Further Developments of the Convection, Viscous Sublayer, and Turbulence Closure Schemes. *Mon. Weather Rev.* **1994**, *122*, 927–945. [CrossRef]
57. Janjić, Z.I. Comments on "Development and Evaluation of a Convection Scheme for Use in Climate Models". *J. Atmos. Sci.* **2000**, *57*, 3686–3686. [CrossRef]
58. Betts, A.K. A new convective adjustment scheme. Part I: Observational and theoretical basis. *Quart. J. Roy. Meteor. Soc.* **1986**, *112*, 677–691. [CrossRef]
59. Betts, A.K.; Miller, M.J. A new convective adjustment scheme. Part II: Single column tests using GATE wave, BOMEX, ATEX and Arctic air-mass data sets. *Q. J. R. Meteorol. Soc.* **1986**, *112*, 693–709. [CrossRef]
60. Huffman, G.; Bolvin, D.; Braithwaite, D.; Hsu, K.; Joyce, R.; Kidd, C.; Nelkin, E.J.; Sorooshian, S.; Tan, C.; Xie, P. *Integrated Multi-Satellite Retrievals for GPM (IMERG), Version 4.4*; NASA's Precipitation Processing Center: Washington, DC, USA, 2014.
61. Hersbach, H.; Dee, D. *ERA5 Reanalysis is in Production*; ECMWF: Reading, UK, 2016.
62. Jones, P. First- and Second-Order Conservative Remapping Schemes for Grids in Spherical Coordinates. *Mon. Weather Rev.* **1999**, *127*, 2204–2210. [CrossRef]
63. Lean, H.W.; Clark, P.A.; Dixon, M.; Roberts, N.M.; Fitch, A.; Forbes, R.; Halliwell, C. Characteristics of High-Resolution Versions of the Met Office Unified Model for Forecasting Convection over the United Kingdom. *Mon. Weather Rev.* **2008**, *136*, 3408–3424. [CrossRef]
64. Beusch, L.; Foresti, L.; Gabella, M.; Hamann, U. Satellite-Based Rainfall Retrieval: From Generalized Linear Models to Artificial Neural Networks. *Remote Sens.* **2018**, *10*, 939. [CrossRef]
65. Sharifi, E.; Eitzinger, J.; Dorigo, W. Performance of the State-Of-The-Art Gridded Precipitation Products over Mountainous Terrain: A Regional Study over Austria. *Remote Sens.* **2019**, *11*, 2018. [CrossRef]
66. Beck, H.; Pan, M.; Roy, T.; Weedon, G.; Pappenberger, F.; van Dijk, A.; Huffman, G.; Adler, R.; Wood, E. Daily evaluation of 26 precipitation datasets using Stage-IV gauge-radar data for the CONUS. *Hydrol. Earth Syst. Sci.* **2019**, *23*, 207–224. [CrossRef]
67. Dezfuli, A.; Ichoku, C.; Huffman, G.; Mohr, K.; Selker, J.; van de Giesen, N.; Hochreutener, R.; Annor, F. Validation of IMERG precipitation in Africa. *J. Hydrometeorol.* **2017**, *18*. [CrossRef]
68. Chu, Q.; Xu, Z.; Chen, Y.; Han, D. Evaluation of the ability of the Weather Research and Forecasting model to reproduce a sub-daily extreme rainfall event in Beijing, China using different domain configurations and spin-up times. *Hydrol. Earth Syst. Sci.* **2018**, *22*, 3391–3407. [CrossRef]
69. Ma, L.M.; Tan, Z.M. Improving the behavior of the cumulus parameterization for tropical cyclone prediction: Convection trigger. *Atmos. Res.* **2009**, *92*, 190–211. [CrossRef]
70. Shepherd, T.; Walsh, K. Sensitivity of hurricane track to cumulus parameterization schemes in the WRF model for three intense tropical cyclones: Impact of convective asymmetry. *Meteorol. Atmos. Phys.* **2017**, *129*. [CrossRef]
71. Bonekamp, P.N.J.; Collier, E.; Immerzeel, W.W. The Impact of Spatial Resolution, Land Use, and Spinup Time on Resolving Spatial Precipitation Patterns in the Himalayas. *J. Hydrometeorol.* **2018**, *19*, 1565–1581. [CrossRef]
72. Kanase, D.R.; Deshpande, M.; Phani, M.K.; Mukhopadhyay, P. Evaluation of convective parameterization schemes in simulation of tropical cyclones by Climate Forecast System model: Version 2. *J. Earth Syst. Sci.* **2020**, *129*. [CrossRef]

73. Reddy, V.; Prasad, S.; Krishna, M.; Reddy, K. Effect of cumulus and microphysical parameterizations on JAL cyclone prediction. *Indian J. Radio Space Phys.* **2014**, *43*, 103–123.

74. Fahad, A.A.; Tanvir, A. Impacts of different cumulus physics over south Asia region with case study tropical cyclone Viyaru. *arXiv* **2015**, arXiv:1506.01481.

75. Biswas, M.; Bernardet, L.; Dudhia, J. Sensitivity of hurricane forecasts to cumulus parameterizations in the Hurricane Weather Research and Forecasting (HWRF) model. *Geophys. Res. Lett.* **2014**, *41*. [CrossRef]